Changes in glacier dynamics in the northern Antarctic Peninsula since 1985

Thorsten Seehaus[1], Alison J. Cook[2], Aline B. Silva[3], Matthias Braun[1]

[1] Institute of Geography, Friedrich-Alexander-University Erlangen-Nuremberg, Wetterkreuz 15, 91058 Erlangen, Germany

[2] Department of Geography, Durham University, South Road, Durham DH1 3LE, United Kingdom

[3] Laboratório de Monitoramento da Criosfera, Universidade Federal do Rio Grande, Av. Itália, km 8, 96203-900, Rio Grande - RS Brazil

Correspondence to: Thorsten Seehaus (*thorsten.seehaus@fau.de*)

Abstract. The climatic conditions along the northern Antarctic Peninsula have shown significant changes within the last 50 years. Here we present a comprehensive analysis of temporally and spatially detailed observations of the changes in ice dynamics along both the east and west coastlines of this region. Temporal trends of glacier area (1985-2015) and ice surface velocity (1992-2014) are derived from a broad multi-mission remote sensing database for 74 glacier basins on the northern Antarctic Peninsula (<65° S along the west coast and north of the Seal Nunataks on the east coast). A recession of the glaciers by 238.81 km² is found for the period 1985-2015, of which the glaciers affected by ice shelf disintegration showed the largest retreat by 208.59 km². Glaciers on the east coast north of the former Prince Gustav Ice Shelf extent in 1986 receded by only 21.07 km² and decelerated by about 69 % on average (1985-2015). A dramatic acceleration after ice shelf disintegration with a subsequent deceleration is observed at most former ice shelf tributaries on the east coast, combined with a significant frontal retreat. In 2014, the flow speed of the former ice shelf tributaries was 16.8 % higher than at the beginning of the study period. Along the west coast the average flow speeds of the glaciers increased by 41.5 %. However, the glaciers on the western Antarctic Peninsula revealed a strong spatial variability of the changes in ice dynamics. By applying a hierarchical cluster analysis we show that this is associated with the geometric parameters of the individual glacier basins. The heterogeneous pattern of ice dynamic trends at the northern Antarctic Peninsula shows that temporally and spatially detailed observations as well as further monitoring are necessary to fully understand glacier change in regions with such strong topographic and climatic variances.

1 Introduction

During the last century, the Antarctic Peninsula (AP) has undergone significant warming (Carcass et al., 1998; Turner et al., 2005), leading to substantial glaciological changes. Skvarca et al. (1998) reported a significant increase in surface air temperatures at the north-eastern AP in the period 1960-1997 and correlated it with the recession of the Larsen and Prince-Gustav Ice shelves (Fig. 1) and the observed retreat of tidewater glaciers on James Ross Island in the period 1975-1995 (Skvarca et al., 1995). However, a recent cooling trend on the AP was revealed by Oliva et al. (2017) and Turner et al.

(2016) since the late 1990s. Shepherd et al. (2012) compiled a comprehensive glacier mass balance database of the polar ice sheets. The authors estimated a mass loss on the whole AP (<73° S) of -36±10 Gt a-1 for the period 2005-2010, which corresponds to 35% of the total mass loss of Antarctica. A projection of sea level rise contribution by the AP ice sheet amounts to 7-16 mm sea-level equivalent by 2100 and 10-25 mm by 2200 (Barrand et al., 2013a). However, along the western AP and on the higher elevation regions an increase in snow accumulation in the late 20th century was derived from ice cores (e.g. at Palmer Land, 73.59° S, 70.36° W, Thomas et al., 2008; Detroit Plateau, 64.08°S, 59.68° W, Potocki et al., 2011; at Bruce Plateau, 66.03°S, 64.07°W, Goodwind, 2013) and climate models (e.g. Dee et al., 2011), whereas van Wessem et al. (2016) obtained insignificant trends in precipitation.

Numerous ice shelves along the AP (e.g. Larsen A/B, Prince Gustav and Wordie) have retreated widely or disintegrated in recent decades (Cook and Vaughan, 2010). As a consequence to the reduced buttressing, former tributary glaciers showed increased ice discharge and frontal retreat (e.g. De Angelis and Skvarca, 2003; Rack and Rott, 2004; Rignot et al., 2004; Seehaus et al., 2015; Wendt et al., 2010). For the northern AP (<66° S), a mass loss rate of -24.9±7.8 Gt a-1 was reported by Scambos et al. (2014) for the period 2003-2008, indicating that major ice mass depletion happened at the northern part of the peninsula, especially along the eastern side where numerous glaciers have been affected by ice shelf collapses. Seehaus et al. (2015, 2016) quantified the ice loss of former ice shelf tributaries. Mass loss rates of -2.14±0.21 Gt a^{-1} (1995-2014) and -1.16±0.16 Gt a^{-1} (1993-2014) were found at Dinsmoor-Bombardier-Edgeworth Glacier System and Sjögren-Inlet glaciers, respectively. Glaciers that were not terminating in an ice shelf also showed considerable changes. Cook et al. (2005, 2014) have analyzed the variations of tidewater glacier fronts since the 1940s. The authors reported that 90% of the observed glaciers retreated, which they partly attributed to atmospheric warming. A more recent study revealed a mid-ocean warming along the southwestern coast of the AP, forcing the glacier retreat in this region (Cook et al., 2016). Pritchard and Vaughan (2007) observed an acceleration of ice flow by ~12% along the west coast of the AP (1995-2005) and linked it to frontal retreat and dynamic thinning of the tidewater glaciers. Observations by Kunz et al. (2012) support this supposition. The authors analyzed surface elevation changes of 12 glaciers on the western AP based on stereoscopic digital elevation models (DEM) over the period 1947-2010. Frontal surface lowering was found at all glaciers, whereas area-wide surface lowering was observed on the north-eastern AP by various author groups (e.g. Berthier et al., 2012; Rott et al., 2014; Scambos et al., 2004; Wuite et al., 2015) as a consequence to ice shelf disintegration.

The collected observations suggest that the ice masses on the AP are contributing to sea level rise and show that glaciers' response to climate change on the AP is not homogeneous and that more detailed knowledge of various aspects on the glacier changes are required. Previous studies often only cover a specific period or region, or focus on one particular aspect of glacier change. Therefore, we study the changes in glacier extent in combination with detailed investigations on ice dynamics as well as other derived geometrical attributes of glaciers on the northern AP (<65° S along the west coast and north of the Seal Nunataks on the east coast, Fig. 1b colored polygons) between 1985 and 2015. We analyze various multi-mission remote sensing datasets in order to obtain methodologically consistent and temporally detailed time series of ice dynamic trends of 74 glacier basins. The observations are individually discussed for the sub regions, considering the different atmospheric, glaciological and oceanic conditions and changes.

2 Study site

The AP is the northern-most region of Antarctica. It covers only 3% of the entire continent in area, but receives 13% of the total mass input (van Lipzig et al., 2002, 2004). The AP's mountain chain (typically 1500-2000 m high) acts as an orographic barrier for the circumpolar westerly air streams leading to very high precipitation values on the west coast and on the plateau region of up to 5000 mm we yr -1, as well as frequent foehn type wind occurrences on the east coast (Cape et al., 2015, Marshall et al., 2006, van Wessem et al. 2016). The foehn events are characterized by strong winds and high air temperatures. Consequently, the climatic mass balance (b_{clim}) shows a strong gradient across the mountain chain (Turner, 2002; van Wessem et al., 2016). Aside from those that are ice shelf tributaries, almost all glaciers on the AP are marine terminating, and the majority of the glacier catchments extend up to the high elevation plateau regions. Typically the AP plateau is separated from the outlet glaciers by escarpments and ice-falls. Glaciers on the west coast drain into the Bellingshausen Sea and on the east coast into the Weddell Sea. Since the 1980s, the ice shelves along the east coast have substantially recessed and disintegrated (Larsen Inlet in 1987-89, Prince Gustav and Larsen A in 1995 and Larsen B in 2002) (Cook and Vaughan, 2010; Skvarca et al., 1999), which Scambos et al. (2003) attributed to higher summer air temperatures and surface melt. A more recent study by Holland et al. (2015) discovered that significant thinning of the Larsen C Ice Shelf is caused by basal melting and that ungrounding from an ice rise and frontal recession could trigger its collapse. The northern AP has a maritime climate and is the only region of Antarctica that frequently experiences widespread surface melt (Barrand et al., 2013b; Rau and Braun, 2002).

Our study site stretches approximately 330 km from the northern tip of the AP mainland southwards to Drygalski Glacier on the east coast and Grubb Glacier on the west coast (Fig. 1). This facilitates the analyses of the long-term response (~20 years) of tributary glaciers to ice shelf disintegration at the former Larsen A and Prince-Gustav ice shelves on the east coast, the investigation of glaciers north of the former Prince-Gustav Ice Shelf, where no information on change in ice flow is currently available, and the comparison with temporal trends in ice dynamics along the west coast at the same latitude. The study region covers an area of ~11,000 km² with altitudes stretching from sea level up to 2220 m. The glacier basin delineations are based on the Antarctic Digital Database ADD 6.0 (Cook et al., 2014). Glacier names are taken from the Global Land Ice Measurements from Space (GLIMS) project database. The local GLIMS glacier IDs (e.g. TPE62, LAB2) are used for unnamed glaciers and further missing glacier basin names are substituted with the ADD 6.0 glacier IDs. Neighboring basins with coalescing ice flow at the termini are merged (many are already merged in the ADD 6.0), as the delineation of the individual glacier sections is not always possible and the width can vary temporally (due to changes in mass flux of the individual glaciers). In these cases, the names of the glaciers are also merged (e.g. Sikorsky-Breguet-Gregory – SBG, see Table 1 for abbreviations of glacier names). Due to the sparse data coverage (fewer than three good quality velocity measurements), no time series analysis of the glaciers at the northern tip of the AP or at some capes and peninsulas (e.g. Sobral Peninsula, Cape Longing) is possible. Therefore, the northern-most analyzed catchments are Broad-Valley Glacier on the east coast and TPE8 Glacier on the west coast, resulting in 74 studied glacier basins. Furthermore, the study region is divided into three sectors, taking into account the different climatic settings and drainage orientation as well as former ice shelf extent: sector "West" - Glaciers on the west coast, draining into the Bransfield and Gerlache Strait; sector "East" – Glaciers on the east coast, draining into the Prince Gustav Channel; and sector "East-Ice-Shelf" – Glaciers on the east coast, that were former tributaries to the Larsen A, Larsen Inlet and Prince Gustav Ice Shelf.

3 Data & Methods

A large number of various remote sensing datasets are analyzed in order to obtain temporally and spatially detailed information on changes in ice dynamics in the study area. Glacier area changes are derived from satellite and aerial imagery. Repeat-pass Synthetic Aperture Radar (SAR) satellite acquisitions are used to compute surface velocity fields in order to obtain information on changes in glacier flow speed. Auxiliary data from sources such as a digital elevation model and glacier inventory are included in the further analyses and discussion of the results.

3.1 Area changes

Changes in glacier area are derived by differencing glacier outlines from various epochs. All observed glaciers are tidewater glaciers and only area changes along the calving front were considered. Information on the positions of the glacier fronts in the study region are taken from Cook et al. (2014), and are available for the whole AP in the ADD 6.0 (1945-2010). This coastal-change inventory is based on manually digitized ice front positions using imagery from various satellites (e.g. Landsat, ERS) and aerial photo campaigns. This dataset is updated (up to 2015) and gaps are filled by manual mapping of the ice front positions based on SAR and optical satellite images. Consistent with Cook et al. (2014), the ice-front positions are assigned to 5-year intervals in order to analyze temporal trends in glacier area changes in the period 1985-2015. Before 1985, only sparse information on ice front positions for the whole study region is available, and the coverage by SAR data for analyzing glacier flow starts in 1992. Additionally, the analysis of the area changes for the Larsen A and Prince Gustav Ice Shelf tributaries is limited to the period 1995-2015, as the ice shelves disintegrated in 1995.

The uncertainties of the glacier change measurements strongly depend on the specifications of the imagery used (e.g. spatial resolution, geodetic accuracies) as well as the methods used. To each record in the coastal-change inventory from the ADD 6.0, a reliability rating is assigned according to Ferrigno et al. (2006). The rating ranges from 1 to 5 (reliability within 60 m to 1 km) and takes into account errors due to manual digitization and interpretation (see Ferrigno et al., 2006 for a detailed description). This approach is also applied on the updated ice-front positions. Nearly all mapped ice fronts in the study region have a good reliability rating of 1 (76%) and 2 (21%). Only a few glacier fronts (3%) have a rating of 3. No ice fronts with reliability ratings of 4 and 5 are mapped in the study area.

3.2 Surface velocities

Surface velocity maps are derived from repeat-pass Synthetic Aperture Radar (SAR) acquisitions. SAR image time series of the satellite missions ERS-1/2, Envisat, RadarSAT-1, ALOS, TerraSAR-X (TSX) and TanDEM-X (TDX) are analyzed, covering the period 1992-2014. Specifications of the SAR sensors are listed in Table 2. The large number of SAR images was provided by the German Aerospace Center (DLR), the European Space Agency (ESA) and the Alaska Satellite Facility (ASF). To obtain displacement fields for the glaciers, the widely used and well approved intensity offset tracking method is applied on co-registered single look complex SAR image pairs (Strozzi et al., 2002). In order to improve the co-registration of the image pairs, we mask out fast moving and unstable regions such as outlet glaciers and the sea during the co-registration processes. Furthermore, single SAR image tiles acquired during the same satellite flyover are concatenated in the along-track direction. This helps to further improve the co-registration in coastal regions (by including more stable areas in the co-registration process) but also simplifies the analysis of the final results as no mosaicking of the results is needed. Image pairs with low quality co-registration are filtered out. A moving window technique is used by the intensity offset tracking method to compute the cross-correlation function of each image patch and to derive its azimuth and slant range displacement. Less reliable offset measurements are filtered out by means of the signal-to-noise ratio of the normalized cross-correlation function. Moreover, we apply an additional filter algorithm based on a comparison of the magnitude and alignment of the displacement vector relative to its surrounding offset measurements. This technique removes more than 90% of incorrect measurements (Burgess et al., 2012). Finally, the displacement fields are transferred from slant range into ground range geometry, taking into account the effects on the local incidence angle by the topography. The results are then geocoded, orthorectified and converted into velocity fields (with 100m pixel spacing for all sensors) by means of the time span between the SAR acquisitions. The mean date of the consecutive SAR acquisitions is assigned to each velocity field. The ASTER Global Digital Elevation Model of the Antarctic Peninsula (AP-DEM, Cook et al., 2012) is used as elevation reference. It has a mean elevation bias of -4 m (±25m RMSE) from ICESat data and horizontal accuracy better than 2 pixels. It is currently the best available digital elevation model of the Antarctic Peninsula.

Depending on the displacement rate and resolution of the SAR sensor, the tracking window size needs to be adapted (de Lange et al. 2007). For the fast flowing central glacier sections, larger window sizes are needed since large displacements cannot be tracked by using small correlation patches. Small tracking window sizes are suitable for the slow moving lateral sections of the outlet glaciers. Wide parts of large tracking patches cover the stable area next to the glacier, which biases the tracking results towards lower velocities. Consequently, we compute surface velocity fields of the same image pairs for different correlation patch sizes in order to get the best spatial coverage. Table 2 shows the different tracking window sizes for each sensor. The results of each image pair are stacked by starting with the results of smallest tracking window size and filling the gaps with the results of the next biggest tracking window size.

The accuracy of the velocity measurements strongly depends on the coregistration quality and the intensity offset tracking algorithm settings. The mismatch of the coregistration ${\sigma_v}^C$ is quantified by measuring the displacement on stable reference areas close to the coast line, such as rock outcrops and nunataks. Based on the Bedmap2 (Fretwell et al., 2013) and ADD 6.0 rock outcrop masks, reference areas are defined and the median displacements magnitude of each velocity field is measured at these areas. The uncertainty of the tracking process ${\sigma_v}^T$ is estimated according to McNabb et al. (2012) and Seehaus et al. (2015) depending on accuracy of the tracking algorithm *C*, image resolution *dx*, oversampling factor *z*, time interval *dt*.

$$\sigma_v^T = \frac{Cdx}{zdt} \tag{1}$$

The accuracy of the tracking algorithm is estimated to be 0.2 pixels and an oversampling factor z=2 is applied to tracking patches in order to improve the accuracy of the tracking process. Both independent error estimates are quadratically summed to compute the uncertainties of the individual velocity fields σ_v.

$$\sigma_v = \sqrt{(\sigma_v^T)^2 + (\sigma_v^C)^2} \tag{2}$$

A profile is defined (red lines in Fig. 1) close to the terminus of each glacier basin, behind the maximum retreat state of ice front position in the observation period. The results are visually inspected in order to remove unreliable measurements, based on the magnitude and direction of ice flow along the profiles. Datasets with partial profile coverage or large data gaps, as well as those with still remaining tracking errors, are rejected. The changes in the ice flow of each glacier are analyzed by measuring the surface velocities along the profiles. In order to reduce the number of data gaps along the profile due to pixel size data voids in the velocity fields, the velocity data is extracted within a buffer zone of 200 m around the profiles. To minimize the impact of potential outliers, median velocities along the profiles are calculated and the temporal trends are plotted. The glaciers are manually classified in six categories according to the temporal evolution of the ice flow speeds (see Table 3), since automatic classification attempts did not succeed. Only glaciers with three or more observations and an observation period of more than 10 years are considered in the categorization, resulting in 74 categorized glacier basins (colored polygons in Fig. 1b. There is a minimum of seven velocity measurements per categorized basin and the shortest observation period is 14.83 years (see Table S1; average number of velocity measurements per glacier is 33.8 and average observation period is 19.40 years). The GAMMA Remote Sensing software is used for processing of the SAR data.

3.3 Catchment geometries and settings

Glacier velocities and area change measurements provide information on the ice dynamics of the individual glaciers. To facilitate a better and comprehensive interpretation of these observations, additional attributes regarding the different geometries and settings of the glaciers are derived. In addition to glacier attributes derived by Huber et al. (2017), we calculated the Hypsometric Index and the ratio of the flux gate cross section divided by the glacier catchment area.

Mass input strongly affects the dynamics of a glacier. The climatic mass balance at the northern AP shows a strong spatial variability, with very high accumulation rates along the west coast, significantly lower values on the east coast and an increase towards higher altitudes along both coast lines (Turner, 2002; van Wessem et al. 2016). Consequently, the mass input depends on the elevation range and the hypsometry. For each glacier basin a Hypsometric Index (*HI*), defined by Jiskoot et al. (2009), is calculated by means of surface elevations from the AP-DEM. Based on this index the glaciers are grouped into the five categories according to Jiskoot et al. (2009), ranging from very top-heavy to very bottom heavy (Table 4). Moreover, the maximum elevations of the individual glacier catchments are derived from the AP-DEM, which represents the altitude range of the catchment, since all observed glaciers are marine terminating.

In order to characterize the catchment shape, the ratios (*FA)* of the flux gate cross sections divided by the glacier catchment areas are calculated. The flux gates are defined along the profiles used for the glacier flow analysis (Section 3.2). Lower values of *FA* indicate a channelized outflow (narrowing towards the glacier front), whereas higher *FA* ratios imply a broadening of the glacier towards the calving front. Ice thickness at the flux gates is taken from the AP Bedmap dataset from Huss and Farinotti (2014).

3.4 Cluster analysis

The glaciers in the sector "West" (Fig. 1, red shaded area) show a heterogeneous pattern of ice dynamics as compared to the other sectors changes (Section 4.1, 4.2). In order to analyze the influence of the glacier geometries on the glaciological changes and to find similarities, a cluster analysis is carried out in sector "West". Variables of the glacier dynamics used are the derived area changes (in percent) and velocity changes (ratings of the categories, Table 3). The glacier geometry parameters used are the Hypsometric Indexes *HI*, maximum surface elevation h_{max} of the basin and the flux gate to catchment size ratio *FA*. The variables are standardized in the traditional way of calculating their standard scores (also known as z-scores or normal scores). It is done by subtracting the variables mean value and dividing by its standard deviation (Miligan and Cooper, 1988). Afterwards a dissimilarity matrix is calculated using the Euclidean distances between the observations (Deza and Deza, 2009). A hierarchical cluster analysis (Kaufman and Rousseeuw, 1990) is applied on the dissimilarities using Ward's minimum variance method (Ward, 1963). At the start, for each glacier a cluster is defined and then the most similar clusters are iteratively joined until only one cluster is left. The distances between the clusters are updated in each iteration step by applying the Lance-Williams algorithms (Lance and Williams, 1967).

4 Results

4.1 Area changes

Area changes relative to the measurements in the epoch 1985-1989 of all observed glaciers are plotted in Fig. S1-S74 (supplement). The glaciers are classified in three groups based on the latest area change measurements, which are illustrated in Fig. 2: retreat (Fig. 2a, b, c, f) – loss of glacier area by frontal retreat; stable (Fig. 2e) – no significant area changes (within the error bars); advance (Fig. 2d) – gain of glacier area by frontal advance. In Fig. 3 the spatial distribution of the area change classification is illustrated. All glaciers along the east coast, including the former ice shelf tributaries, retreated, whereas along the west coast, numerous glaciers show stable ice front positions and some glaciers even advanced. In total, 238 km² of glacier area was lost in the study region in the period 1985-2015, which corresponds to a relative loss of 2.2%. All sectors show glacier area loss (Table 5), of which the area loss by 5.7% at sector "East-Ice-Shelves" clearly dominates. The glaciers in sector "West" and "East" recessed by 0.2% and 1.4%, respectively. The temporal trends of total glacier area and area loss of all observed glaciers and of each sector are presented in Fig. 4. Catchment areas and changes between 1985 and 2015 of the individual basins are listed in Table S1 (supplement) and relative changes are illustrated in Fig. 5.

4.2 Surface velocities

A total of 282 stacked and filtered velocity fields are derived from the SAR acquisitions covering the period from 25th December, 1992 until 16th December, 2014. The average total uncertainty of the velocity fields amounts to 0.08 ± 0.07 m d^{-1} and the values for each SAR sensor are provided in Table 2. In Table S2 (supplement) the error estimates of each velocity field are listed. The mean sample count to estimate the coregistration quality is 11717 and the average mismatch amounts to 0.07 m d^{-1}. The error caused by the tracking algorithm strongly varies depending on the source of the SAR data (sensor). A mean value of 0.05 m d^{-1} is found. ERS image pairs with time intervals of one day have very large estimated tracking uncertainties, biased by the very short temporal baselines. Therefore, only the errors caused by the mismatch of the coregistration are considered in the total error computations of the seven ERS tracking results with one day temporal baselines.

All measured velocity profiles of the 74 observed glaciers are visually inspected and in total 2503 datasets passed the quality check (on average ~34 per glacier). Figure 2 shows by example the temporal evolution of the ice flow for each velocity change category (see Table 3). The temporal trends of the surface velocities at the termini of each glacier are plotted in Fig. S1-S74 (supplement) and the related categories are listed in Table S1 (supplement). The spatial distribution of the categories is illustrated in Fig. 3. At nearly all glaciers in sector "East-Ice-Shelf" a peak in ice velocities is observed. In the sector "East", most glaciers showed a decrease in flow velocities in the observation period. The glaciers on the west coast show a more irregular distribution than along the east coast, but a local clustering of accelerating glaciers can be observed at Wilhelmina Bay.

For each glacier the flow velocities in the first v_S and last year v_E of the observation period as well as the absolute and relative change dv is presented in Table S1 (supplement). The mean values of v_S, v_E and dv of all analyzed glaciers and for each sector are listed in Table 5. On average the ice flow in the study region increased by 1.6%, but the glaciers in the individual sectors showed on average significant change. Along the west coast an average acceleration by 41.5% occurred and the former ice shelf tributaries on the east coast accelerated by 16.8%. In the sector "East" the glaciers decelerated resulting in a mean velocity change of -69%. The presented average flow speed change values are based on the observed changes of all glaciers in the respective sector (Table S1), ignoring the different size of the individual glaciers. The shortest observation period is 14.83 years at DBC31 Glacier, the longest observation period is 21.99 years at TPE31 and Sjögren glaciers and on average velocity changes are analyzed over a period of 19.40 years (σ = 1.97 years).

4.3 Catchment geometries and settings

The spatial distribution of Hypsometric Indexes and categories of the glacier basins is presented in Fig. 3 and the values are listed in Table S1 (supplement). The HI values range between -4.6 and 9.1 (mean: 0.88, σ: 2.10). No clear spatial distribution pattern can be identified, reflecting the heterogeneous topography of the AP. The maximum elevation of the catchments and the *FA* factors are also listed in Table S1 (supplement).

4.4 Cluster analysis

The resulting dendrogram of the hierarchical cluster analysis is plotted in Fig. 6. Four groups are distinguished. The boxplots of each input variable are generated based on this grouping and are shown in Fig. 7. The characteristics of the groups are discussed in Section 5.3.

5 Discussion

Most of the observed glaciers (62%) retreated and only 8% advanced in the study period. These findings are comparable to the results of Cook et al. (2005, 2014, 2016). Only glaciers along the west coast showed stable or advancing calving fronts and all glaciers on the east coast receded since 1985. This heterogeneous area change pattern was also observed by Davies et al. (2012) on western Trinity Peninsula. Most significant retreat occurred in the sector "East-Ice-Shelf". In the period 1985-1995, the Larsen Inlet tributaries (APPE-glaciers) lost 45.0 km² of ice. After the disintegration of Prince-Gustav and Larsen A Ice Shelf, the tributaries rapidly retreated in the period 1995-2005. The recession slowed down in the latest observation interval (2005-2010). This trend is comparable to detailed observations by Seehaus et al. (2015, 2016) at individual glaciers (DBE glaciers and Sjögren-Inlet glaciers). At sector “East” the highest area-loss is found in the earliest observation interval (1985-1990). Davies et al. (2012) also reported higher shrinkage rates for most of the glaciers in this sector in the period 1988-2001 than in the period 2001-2009. Moreover, slightly increased recession is also found in the time period (1995-2005, Fig. 4) at sector “East”. Davies et al. (2012) and Hulbe et al. (2004) supposed that the disintegration of an ice shelf affects the local climate. The air temperatures would rise due to the presence of more ice free water in summers. This might explain the slightly higher retreat rates at sector “East”. At Base Marambio, ~100 km east of this sector, approximately 2°C higher mean annual air temperatures were recorded in the period 1996-2005 as compared to the period 1986-1995 (Oliva et al., 2017). Unfortunately, no temperature data recorded within sector “East” is available covering this period that could be used to validate this theory.

The average changes of flow velocities at each sector also vary strongly (Table 5) in the observation period 1992-2014. On the west coast an increase of 42% is found, whereas in sector “East” the glaciers slowed down by approximately 69% and at the ice shelf tributaries the ice flow increased on average by 17%. Pritchard and Vaughan (2007) reported an increase in mean flow rate of 7.8% in frame 4923 (the central and much of the northern part of sector “West”) and 15.2% in frame 4941 (the southern part of sector “West”) for the period 1992-2005 (frame numbers correspond to European Space Agency convention for identifying ERS coverage). This spatial trend corresponds to our observations, since most of the glaciers with a clear positive velocity trend are located at the southern end of sector “West”. However, for the same observation period we derived a mean increase in flow velocity by 18.9 % in sector “West”, which is an approximately 1.6 times higher acceleration. Pritchard and Vaughan (2007) estimated the mean velocity change by measuring the flow speed at profiles along the flow direction of the glacier, whereas we measured the velocity across glacier profiles at the terminus. If a tidewater glacier speeds up due to the destabilization of its front, the highest acceleration is found at the terminus (see Seehaus et al., 2015, Fig. 3). Consequently, the different profile locations explain the deviations between both studies.

In the following section the observed changes in the individual sectors are discussed in more detail.

5.1 East

The glaciers north of the former Prince-Gustav Ice Shelf show a general trend towards lower flow velocities. Eyrie, Russell East, TPE130, TPE31, TPE32, TPE34, and “2731” glaciers experienced a rapid decrease and, except “2731” Glacier, a subsequent stabilization or even gentle acceleration of flow velocities (Fig. S2, S6, S7 and S9-S12). A significant retreat followed by a stabilization or slight re-advance of the calving front position is also observed at these glaciers. According to Benn and Evans (1998), a small retreat of a glacier with an overdeepening behind its grounding line (i.e. where the bed slopes away from the ice front) can result in a rapid recession into the deepening fjord. The increased calving and retreat of the ice front cause stronger up-glacier driving stress, higher flow speed as well as glacier thinning and steepening (Meier and

Post, 1987; Veen, 2002). The glacier front stabilizes when the grounding line reaches shallower bathymetry and ice flow also starts to slowdown. A delay between the front stabilization and slowdown can be caused by thinning and steepening of the glacier. Additionally, the accelerated ice flow can surpass the retreat rates and cause short-term glacier advances in the period of high flow speeds (e.g. Eyrie, Russel East, TPE130 and TPE32 glaciers, Fig. S6, S7, S9 and S11) (Meier and Post, 1987). This process can be initiated by climatic forcing (Benn and Evans, 1998). Significant higher surface air temperature at the north-eastern AP and a cooling trend in the 21st century was reported by Oliva et al. (2017), Skvarca et al. (1998) and Turner et al. (2016) (see Section 1). Hence, we assume that the initial recessions of the glaciers in sector “East” were forced by the warming observed by Oliva et al. (2017) and Skvarca et al. (1998) since the 1970s. Therefore, this initial frontal destabilization and retreat led to high flow speeds at the beginning of our ice dynamics time series (earliest velocity measurements from 1992) and the subsequently observed frontal stabilization (after 1985) caused the deceleration of the ice flow. The fjord geometry significantly affects the dynamics of the terminus of a tidewater glacier (Benn and Evans, 1998; van der Veen, 2002). The tongues of Aitkenhead and “2707” glaciers are split into two branches by nunataks, resulting in rather complex fjord geometries. A retreat from pinning points (e.g. fjord narrowing) causes further rapid recession and higher flow speeds until the ice front reaches a new stable position as observed at “2707” and Aitkenhead Glacier (Fig. S1 and S3). At TPE10 Glacier (Fig. S8) a “peaked” flow velocity trend is observed as at Aitkenhead Glacier. No nunatak is present at the terminus, but small rock outcrops, indicating a shallow bedrock bump, are identified north of the center of the ice front by visual inspection of optical satellite imagery. Most probably, this shallow bedrock acts as a pinning point and prevents further retreat. The front of Broad Valley Glacier (Fig. S4) is located in a widening fjord. This geometry makes the glacier less vulnerable to frontal changes (Benn and Evans, 1998). Therefore, no significant changes in flow velocities are observed as a consequence of the frontal recession and re-advance.

Diplock and Victory glaciers (Fig. S5 and S13) show a decrease of flow speed during retreat followed by an acceleration combined with frontal advance. Surge-type glaciers, found for example in Alaska (tidewater) (Motyka and Truffer, 2007; Walker and Zenone, 1988) or Karakoram (land terminating) (Rankl et al., 2014), show similar behavior. They are characterized by episodically rapid down-wasting, resulting in a frontal acceleration and strong advance. Regarding tidewater glaciers the advance can be strongly compensated by increased calving rates in deepwater in front of the glacier. It is therefore possible that these glaciers may have experienced a surge cycle in our observation period; however, a longer time series analysis is necessary to prove this hypothesis.

5.2 East-Ice-Shelf

In the sector “East-Ice-Shelf” the tributary glaciers in the Larsen A embayment (“2558”, Arron Icefall, DBE, Drygalski, LAB2, LAB32, TPE61 and TPE62; Fig. S14, S17, S19-S22, S25 and S26) and Sjögren-Inlet (Boydell, Sjögren and TPE114; Fig. S18, S23 and S24) lost the downstream ice shelves in 1995. Nearly all glaciers showed a rapid and significant acceleration after ice shelf break up and a subsequent slow down. A gentle peak in flow speeds is obtained at LAB32 and TPE114 glaciers. They are classified as “stable”, since the variations are below the threshold of 0.25 m d^{-1}, according to the categorization in Table 3. Dramatic speed up with subsequent deceleration of former ice shelf tributaries was reported by various authors; e.g. in this sector by Seehaus et al., (2015, 2016) at DBE and Sjögren-Inlet glaciers and further south at Larsen B embayment by Rott et al. (2011) and Wuite et al. (2015). The velocities reported by Rott et al. (2014) at Sjögren, Pyke, Edgeworth and Drygalski glaciers are generally higher than our findings. The authors measured the velocities at locations near the center of the glacier fronts, where the ice flow velocities are typically highest, whereas we measured the median velocities at cross profiles close to the glacier fronts (Seehaus et al. 2015). The different approaches result in different absolute values, but comparable temporal trends in glacier flow speeds are observed by both author groups. For example Rott et al. (2015) presented surface velocity measured along a central flow line of Drygalski Glacier. Figure S75 shows our surface velocity measurements across the terminus of Drygalski Glacier. Both studies show comparable values at the center of the terminus.

Highest peak values of 6.3 m d^{-1} are found at TPE61 Glacier in November 1995 and January 1996. Most glaciers (Arron Icefall, Drygalski, LAB2, TPE61, TPE62) decelerated towards pre-collapse values and show almost constant flow speeds in recent years, indicating that the glaciers adjusted to the new boundary conditions. At “2558”, Boydell, DBE and Sjögren glaciers the deceleration is ongoing and Boydell and DBE glaciers still show increased flow speeds at the glacier fronts. We suppose that these tributary glaciers show a prolonged response to ice shelf disintegration, caused by local settings (e.g. bedrock topography or fjord geometry), and are still adjusting to the new boundary conditions, as suggested by Seehaus et al. (2015, 2016).

In the 1980s, Prince Gustav Ice Shelf gradually retreated (see Fig. 1) and “2668” Glacier (Fig. S15) has not been buttressed by the ice shelf since the early 1990s. A deceleration is found in the period 2005-2010. Hence, this glacier may also have experienced a speed up in the early 1990s due to the recession of Prince Gustav Ice Shelf in the 1980s. However, the earliest velocity measurement at “2668” Glacier is only available from February 1996.

The ice shelf in Larsen Inlet disintegrated in 1987-1988 and earliest velocity measurements are obtained in 1993. Therefore, a potential peak in the flow speed after ice shelf break-up cannot be detected at APPE glaciers (Fig. S16). As for “2668” Glacier no sufficient cloud free coverage by Landsat imagery is available which facilitates the computation of surface velocities for the 1980s. The ice flow at APPE glaciers shows a nearly stable trend with short term variations in the order of 0.2-0.5 m d^{-1} between 1993 and 2014. Rott et al., (2014) also found nearly constant flow velocities at Pyke Glacier. The authors suggest that the ice flow of APPE glaciers was not strongly disturbed by the ice shelf removal due to the steep glacier surfaces and shallow seabed topography at the glacier fronts (Pudsey et al., 2001).

5.3 West

Meredith and King (2005) reported an increase of surface summer temperatures by more than 1°C in the ocean west of the AP since the 1950s. The authors attributed this to atmospheric warming and reduced sea ice production rates. However, Cook et al. (2016) reported cool ocean temperatures along the north-western AP for the period 1945-2009, and an absence of the atmospheric warming, especially pronounced at the northern AP, since the turn of the millennium was found by Oliva et al. (2017) and Turner et al. (2016), which correlates with an increase of sea ice concentration and the cool ocean temperatures at the northern AP. Thus, the climatic conditions do not show a spatially and temporally constant trend. Moreover the glacier geometries differ strongly, and especially in the southern part of sector "West", the coastline is more jagged. These factors cause the heterogeneous pattern of area and flow speed changes in sector "West" as compared to the eastern sectors.

Kunz et al. (2012) observed thinning at the glacier termini along the western AP, by analyzing airborne and spaceborne stereo imagery in the period 1947-2010. Two of the twelve studied glaciers are located within our study area; Leonardo Glacier (1968-2010) and Rozier Glacier (1968-2010). An acceleration and terminus retreat can be caused by frontal thinning as shown by Benn et al. (2007). However, Benn et al. (2007) also point out that changes in ice thickness do not necessarily affect the ice flow and that calving front positions and ice dynamics are strongly dependent on the fjord and glacier geometries, derived from modeling results which have higher uncertainties especially for smaller basins.

The large number of glaciers in this sector is analyzed by means of a hierarchical cluster analysis (Section 3.4) and assorted into four groups based on the dissimilarities, resulting in the dendrogram plotted in Fig. 6. Boxplots of the individual input variables of each group are shown in Fig. 7. The correlation between the observed ice dynamics and the glacier geometries of each group are discussed in the following sections (see also Fig. 7).

Group1 (14 glaciers):

Most glaciers experienced acceleration over the study period. The majority of the glacier basins are "very top-heavy" or "top-heavy" (median *HI* = -1.8), stretching from sea level up to 1892 m on average. The b_{clim} increases toward higher altitudes (van Wessem et al., 2016) and highest values are found in regions between 1000 and 1700 m a.s.l.. Consequently these glaciers receive high mass input in their large high altitude accumulation regions. The accumulation is known to have significantly increased on the AP by 20% since 1850 (Thomas et al., 2008). Pritchard and Vaughan (2007) reported that only a small fraction of the acceleration can be attributed to glacier thickening due to increased mass input. Up-glacier thickening combined with frontal thinning (reported by Kunz et al., 2012) leads to a steepening of the glacier and an increase in driving stress, resulting in faster ice flow (Meier and Post, 1987) as observed in this study. Moreover, a thinning of the terminus reduces the effective basal stress of a tidewater glacier and facilitates faster ice flow (Pritchard and Vaughan, 2007). The flux gate cross sections to catchment size ratios are relatively small, indicating narrowing catchments towards the ice front. The channelized increased ice flow almost compensates for the increased calving rates (due to frontal thinning), resulting in an average shrinkage of the glaciers by only 0.2% in the period 1985-2015. The high flow speeds may outweigh the calving and lead to ice-front advances as measured at Krebs and TPE46 Glacier. The glacier termini of this group are typically located in narrow fjords (Fig. 5) and are clustered in Charcot, Charlotte and Andvord Bay.

Group 2 (19 glaciers)

Glaciers of group 2 are spread all over the study region, with a local clustering in Wilhelmina Bay. Group 2 shows similar h_{max} and *FA* characteristics to group 1. Area changes are also quite small (-0.1%). Most of the glaciers experienced positive or "peaked" velocities trends. In contrast to group 1 the catchments are in general "bottom-heavy" and some are even "very bottom-heavy". We assume that the constraints are similar to group 1 (increasing b_{clim}, frontal thinning and steepening). However, the additional mass accumulation in the upper regions is smaller due to the "bottom-heavy" glacier geometries. Consequently, the imbalance due to the frontal thinning and up-glacier mass gain is less pronounced as in group 1 and numerous glaciers ("peak" type) started to decelerate after the speed-up, indicating that these glaciers are adjusting to the new boundary conditions.

Group 3 (13 glaciers)

These basins typically show a "bottom-heavy" hypsometry and smaller elevation ranges (in average up to 1103 m a.s.l.). Thus, b_{clim} is relatively low. The smaller mean ice thickness at the termini (161 m, compared to 211 m of all glaciers) of group 3 implies less interaction with the ocean, leading to a small average frontal retreat of ~0.1%. The low frontal ablation does not significantly affect the ice flow, probably due to the flat glacier topography and the low mass input. Consequently, the flow speed is in general stable or even slightly decreases in the observation period. Glaciers of group 3 usually face the open ocean, and do not terminate in narrow fjords (especially in the northern part, Trinity Peninsula).

Group 4 (3 glaciers)

All basins in this group have a "very bottom-heavy" hypsometry and an elevation range comparable to group 3 glaciers. The *FA* factors are in general higher than in group 3, implying that outflow of the catchments is less channelized and the glacier fronts are long compared to the catchment sizes. Therefore, the largest relative area changes, in average -5.1%, are found at glaciers in group 4. However, the absolute frontal retreat is small and does not significantly affect the glacier flow. Note: Group 4 consists of only three samples, limiting the significance.

6 Conclusions

Our analysis expands on previous work on ice dynamic changes along the west coast of AP between TPE8 and Bagshawe-Grubb Glacier, both in regard to temporal coverage and analysis methods. It also spatially extends previous work on changes in ice dynamics along the east coast between Eyrie Bay and the Seal Nunataks. The spatially and temporally detailed analysis of changes in ice flow speeds (1992-2014) and ice front positions (1985-2015) reveal varying temporal trends in glacier dynamics along the northern AP. The results are in general in line with findings of the previous studies, however along the west coast higher glacier flow was determined and on the eastern side trends in ice dynamics of 21 glaciers were observed for the first time. A large variety of temporal trends in glacier dynamics were observed in our study region and attributed to different forcing and boundary conditions.

On the east side all glacier fronts retreated in the study period (relative to 1985), with highest retreat rates observed at former tributaries of the Prince Gustav, Larsen Inlet and Larsen A ice shelves (relative to the year of ice shelf disintegration). Moreover, nearly all the glaciers affected by ice shelf disintegration showed similar temporal trends of ice velocities. The glaciers reacted with a strong acceleration to ice shelf break up followed by a deceleration, indicating that the glaciers adjusted or are still adjusting to the new boundary conditions. Glaciers on the east coast north of the former Prince Gustav Ice Shelf showed in general a significant deceleration and a reduction in frontal ablation. Based on the observed warming trend since the 1960s and the subsequent cooling since the mid-2000s in the northern AP, we conclude that the initial recession and speed up of the glaciers took place before the start of our observation and that the glaciers are now close to a new equilibrium.

The average flow speed of the glaciers along the west coast of the Antarctic Peninsula significantly increased in the observation period but the total frontal change was negligible. No general pattern is obvious in the ice dynamic changes. However, correlations between the changes in ice dynamics and the glacier geometries of the individual catchments were obtained by applying a hierarchical cluster analysis. Thus, the geometry of the individual glacier basin strongly affects the reaction of the glacier to external forcing.

We conclude that for regions with such a strong spatial variation in topographic and climatic parameters as the AP, it is impossible to derive a regional trend in glacier change by simply analyzing individual glaciers in this region. Therefore further detailed observation of the glaciological changes along the AP is needed. Future activities should link remote sensing derived ice dynamics and glacier extent with ocean parameters and ocean models, as well as regional climate models and ice dynamic models, in order to provide a better quantification of mass changes and physical processes leading to the observed changes.

Author contributions. T.S. designed the study, processed the SAR data, performed the data analysis and led the writing of the manuscript, in which he received support from all authors. A.C. and A.S. compiled and provided glacier front position data sets. MB initiated the project and coordinated the research.

Competing interests. The authors declare no competing financial interests.

Acknowledgements. This work was supported by the Deutsche Forschungsgemeinschaft (DFG) in the framework of the priority programme "Antarctic Research with comparative investigations in Arctic ice areas" by a grant to M.B. (BR 2105/9-1). MB and TS would like to thank the HGF Alliance “Remote Sensing of Earth System Dynamics” (HA-310) and Marie-Curie-Network International Research Staff Exchange Scheme IMCONet (EU FP7-PEOPLE-2012-IRSES) for additional support. Access to satellite data was kindly provided by various space agencies, e.g. under ESA AO 4032, DLR TerraSAR-X Background Mission Antarctic Peninsula & Ice Shelves, TSX AO LAN0013, TanDEM-X Mission TDX AO XTI_GLAC0264, ASF, GLIMS as well as NASA and USGS.

References

Barrand, N.E., Hindmarsh, R.C.A., Arthern, R.J., Williams, C.R., Mouginot, J., Scheuchl, B., Rignot, E., Ligtenberg, S.R.M., Van Den Broeke, M.R., Edwards, T.L., Cook, A.J., Simonsen, S.B., 2013a. Computing the volume response of the Antarctic Peninsula ice sheet to warming scenarios to 2200. J. Glaciol. 59, 397–409. doi:10.3189/2013JoG12J139

Barrand, N.E., Vaughan, D.G., Steiner, N., Tedesco, M., Kuipers Munneke, P., van den Broeke, M.R., Hosking, J.S., 2013b. Trends in Antarctic Peninsula surface melting conditions from observations and regional climate modeling. J. Geophys. Res. Earth Surf. 118, 315–330. doi:10.1029/2012JF002559

Benn, D.I., Evans, D.J.A., 1998. Glaciers & Glaciation. Arnold.

Benn, D.I., Hulton, N.R.J., Mottram, R.H., 2007. “Calving laws”, “sliding laws” and the stability of tidewater glaciers. Ann. Glaciol. 46, 123–130. doi:10.3189/172756407782871161

Berthier, E., Scambos, T.A., Shuman, C.A., 2012. Mass loss of Larsen B tributary glaciers (Antarctic Peninsula) unabated since 2002. Geophys. Res. Lett. 39, L13501. doi:10.1029/2012GL051755Burgess, E.W., Forster, R.R., Larsen, C.F., Braun, M., 2012. Surge dynamics on Bering Glacier, Alaska, in 2008–2011. The Cryosphere 6, 1251–1262. doi:10.5194/tc-6-1251-2012

Cape, M.R., Vernet, M., Skvarca, P., Marinsek, S., Scambos, T., Domack, E., 2015. Foehn winds link climate-driven warming to ice shelf evolution in Antarctica. J. Geophys. Res. Atmospheres 2015JD023465. Doi: 10.1002/2015JD023465

Cook, A. j., Vaughan, D. g., Luckman, A. j., Murray, T., 2014. A new Antarctic Peninsula glacier basin inventory and observed area changes since the 1940s. Antarct. Sci. 26, 614–624. doi:10.1017/S0954102014000200

Cook, A.J., Fox, A.J., Vaughan, D.G., Ferrigno, J.G., 2005. Retreating Glacier Fronts on the Antarctic Peninsula over the Past Half-Century. Science 308, 541–544. doi:10.1126/science.1104235

Cook, A.J., Holland, P.R., Meredith, M.P., Murray, T., Luckman, A., Vaughan, D.G., 2016. Ocean forcing of glacier retreat in the western Antarctic Peninsula. Science 353, 283–286. doi:10.1126/science.aae0017

Cook, A.J., Murray, T., Luckman, A., Vaughan, D.G., Barrand, N.E., 2012. A new 100-m Digital Elevation Model of the Antarctic Peninsula derived from ASTER Global DEM: methods and accuracy assessment. Earth Syst. Sci. Data 4, 129–142. doi:10.5194/essd-4-129-2012

Cook, A.J., Vaughan, D.G., 2010. Overview of areal changes of the ice shelves on the Antarctic Peninsula over the past 50 years. The Cryosphere 4, 77–98. doi:10.5194/tc-4-77-2010

Davies, B.J., Carrivick, J.L., Glasser, N.F., Hambrey, M.J., Smellie, J.L., 2012. Variable glacier response to atmospheric warming, northern Antarctic Peninsula, 1988–2009. The Cryosphere 6, 1031–1048. doi:10.5194/tc-6-1031-2012

De Angelis, H., Skvarca, P., 2003. Glacier Surge After Ice Shelf Collapse. Science 299, 1560–1562. doi:10.1126/science.1077987

de Lange, R., Luckman, A., Murray, T., 2007. Improvement of Satellite Radar Feature Tracking for Ice Velocity Derivation by Spatial Frequency Filtering. IEEE Trans. Geosci. Remote Sens. 45, 2309–2318. doi:10.1109/TGRS.2007.896615

Dee, D.P., Uppala, S.M., Simmons, A.J., Berrisford, P., Poli, P., Kobayashi, S., Andrae, U., Balmaseda, M.A., Balsamo, G., Bauer, P., Bechtold, P., Beljaars, A.C.M., van de Berg, L., Bidlot, J., Bormann, N., Delsol, C., Dragani, R., Fuentes, M., Geer, A.J., Haimberger, L., Healy, S.B., Hersbach, H., Hólm, E.V., Isaksen, L., Kållberg, P., Köhler, M., Matricardi, M., McNally, A.P., Monge-Sanz, B.M., Morcrette, J.-J., Park, B.-K., Peubey, C., de Rosnay, P., Tavolato, C., Thépaut, J.-N., Vitart, F., 2011. The ERA-Interim reanalysis: configuration and performance of the data assimilation system. Q. J. R. Meteorol. Soc. 137, 553–597. doi:10.1002/qj.828

Deza, E., Deza, M.M., 2009. Encyclopedia of Distances. Springer Berlin Heidelberg, Berlin, Heidelberg.

Ferrigno, J.G., Cook, A.J., Foley, K.M., Williams, R.S., Swithinbank, C., Fox, A.J., Thomson, J.W., Sievers, J., 2006. Coastal-change and glaciological map of the Trinity Peninsula area and South Shetland Islands, Antarctica, 1843-2001.

Fretwell, P., Pritchard, H.D., Vaughan, D.G., Bamber, J.L., Barrand, N.E., Bell, R., Bianchi, C., Bingham, R.G., Blankenship, D.D., Casassa, G., Catania, G., Callens, D., Conway, H., Cook, A.J., Corr, H.F.J., Damaske, D., Damm, V., Ferraccioli, F., Forsberg, R., Fujita, S., Gim, Y., Gogineni, P., Griggs, J.A., Hindmarsh, R.C.A., Holmlund, P., Holt, J.W., Jacobel, R.W., Jenkins, A., Jokat, W., Jordan, T., King, E.C., Kohler, J., Krabill, W., Riger-Kusk, M., Langley, K.A., Leitchenkov, G., Leuschen, C., Luyendyk, B.P., Matsuoka, K., Mouginot, J., Nitsche, F.O., Nogi, Y., Nost, O.A., Popov, S.V., Rignot, E., Rippin, D.M., Rivera, A., Roberts, J., Ross, N., Siegert, M.J., Smith, A.M., Steinhage, D., Studinger, M., Sun, B., Tinto, B.K., Welch, B.C., Wilson, D., Young, D.A., Xiangbin, C., Zirizzotti, A., 2013. Bedmap2: improved ice bed, surface and thickness datasets for Antarctica. The Cryosphere 7, 375–393. doi:10.5194/tc-7-375-2013

Goodwin, B.P., 2013. Recent Environmental Changes on the Antarctic Peninsula as Recorded in an ice core from the Bruce Plateau. The Ohio State University.

Holland, P.R., Brisbourne, A., Corr, H.F.J., McGrath, D., Purdon, K., Paden, J., Fricker, H.A., Paolo, F.S., Fleming, A.H., 2015. Oceanic and atmospheric forcing of Larsen C Ice-Shelf thinning. The Cryosphere 9, 1005–1024. doi:10.5194/tc-9-1005-2015

Huber, J., Cook, A.J., Paul, F., Zemp, M., 2017. A complete glacier inventory of the Antarctic Peninsula based on Landsat 7 images from 2000 to 2002 and other preexisting data sets. Earth Syst. Sci. Data 9, 115–131. doi:10.5194/essd-9-115-2017

Hulbe, C.L., MacAyeal, D.R., Denton, G.H., Kleman, J., Lowell, T.V., 2004. Catastrophic ice shelf breakup as the source of Heinrich event icebergs. Paleoceanography 19, PA1004. doi:10.1029/2003PA000890

Huss, M., Farinotti, D., 2014. A high-resolution bedrock map for the Antarctic Peninsula. The Cryosphere 8, 1261–1273. doi:10.5194/tc-8-1261-2014

Jiskoot, H., Curran, C.J., Tessler, D.L., Shenton, L.R., 2009. Changes in Clemenceau Icefield and Chaba Group glaciers, Canada, related to hypsometry, tributary detachment, length–slope and area–aspect relations. Ann. Glaciol. 50, 133–143. doi:10.3189/172756410790595796

Kaufman, L., Rousseeuw, P.J., 1990. Finding groups in data: an introduction to cluster analysis, Wiley series in probability and mathematical statistics. Wiley, New York.

Kunz, M., King, M.A., Mills, J.P., Miller, P.E., Fox, A.J., Vaughan, D.G., Marsh, S.H., 2012. Multi-decadal glacier surface lowering in the Antarctic Peninsula. Geophys. Res. Lett. 39, L19502. doi:10.1029/2012GL052823

Lance, G.N., Williams, W.T., 1967. A general theory of classificatory sorting strategies: II. Clustering systems. Comput. J. 10, 271–277. doi:10.1093/comjnl/10.3.271

Marshall, G.J., Orr, A., van Lipzig, N.P.M., King, J.C., 2006. The Impact of a Changing Southern Hemisphere Annular Mode on Antarctic Peninsula Summer Temperatures. J. Clim. 19, 5388–5404. doi:10.1175/JCLI3844.1

McNabb, R.W., Hock, R., O'Neel, S., Rasmussen, L.A., Ahn, Y., Braun, M., Conway, H., Herreid, S., Joughin, I., Pfeffer, W.T., Smith, B.E., Truffer, M., 2012. Using surface velocities to calculate ice thickness and bed topography: a case study at Columbia Glacier, Alaska, USA. J. Glaciol. 58, 1151–1164. doi:10.3189/2012JoG11J249

Meier, M.F., Post, A., 1987. Fast tidewater glaciers. J. Geophys. Res. Solid Earth 92, 9051–9058. doi:10.1029/JB092iB09p09051

Meredith, M.P., King, J.C., 2005. Rapid climate change in the ocean west of the Antarctic Peninsula during the second half of the 20th century. Geophys. Res. Lett. 32, L19604. doi:10.1029/2005GL024042

Milligan, G.W., Cooper, M.C., 1988. A study of standardization of variables in cluster analysis. J. Classif. 5, 181–204. doi:10.1007/BF01897163

Motyka, R.J., Truffer, M., 2007. Hubbard Glacier, Alaska: 2002 closure and outburst of Russell Fjord and postflood conditions at Gilbert Point. J. Geophys. Res. Earth Surf. 112, F02004. doi:10.1029/2006JF000475

Oliva, M., Navarro, F., Hrbáček, F., Hernández, A., Nývlt, D., Pereira, P., Ruiz-Fernández, J., Trigo, R., 2017. Recent regional climate cooling on the Antarctic Peninsula and associated impacts on the cryosphere. Sci. Total Environ. 580, 210–223. doi:10.1016/j.scitotenv.2016.12.030

Potocki, M., Mayewski, P.A., Kurbatov, A., Handley, M., Simoes, J.C., Jaña, R., 2011. Detailed Glaciochemical Records from a Northern Antarctic Peninsula Site - Detroit Plateau. AGU Fall Meet. Abstr. 43.

Pritchard, H.D., Vaughan, D.G., 2007. Widespread acceleration of tidewater glaciers on the Antarctic Peninsula. J. Geophys. Res. 112. doi:10.1029/2006JF000597

Pudsey, C.J., Evans, J., Domack, E.W., Morris, P., Valle, R.A.D., 2001. Bathymetry and acoustic facies beneath the former Larsen-A and Prince Gustav ice shelves, north-west Weddell Sea. Antarct. Sci. 13, 312–322. doi:10.1017/S095410200100044X

Rack, W., Rott, H., 2004. Pattern of retreat and disintegration of the Larsen B ice shelf, Antarctic Peninsula. Ann. Glaciol. 39, 505–510.

Rankl, M., Kienholz, C., Braun, M., 2014. Glacier changes in the Karakoram region mapped by multimission satellite imagery. The Cryosphere 8, 977–989. doi:10.5194/tc-8-977-2014

Rau, F., Braun, M., 2002. The regional distribution of the dry-snow zone on the Antarctic Peninsula north of 70°S. Ann. Glaciol. 34, 95–100. doi:10.3189/172756402781817914

Rignot, E., Casassa, G., Gogineni, P., Krabill, W., Rivera, A., Thomas, R., 2004. Accelerated ice discharge from the Antarctic Peninsula following the collapse of Larsen B ice shelf. Geophys. Res. Lett. 31. doi:10.1029/2004GL020697

Rott, H., Floricioiu, D., Wuite, J., Scheiblauer, S., Nagler, T., Kern, M., 2014. Mass changes of outlet glaciers along the Nordensjköld Coast, northern Antarctic Peninsula, based on TanDEM-X satellite measurements. Geophys. Res. Lett. 2014GL061613. doi:10.1002/2014GL061613

Rott, H., Müller, F., Nagler, T., Floricioiu, D., 2011. The imbalance of glaciers after disintegration of Larsen-B ice shelf, Antarctic Peninsula. The Cryosphere 5, 125–134. doi:10.5194/tc-5-125-2011

Rott, H., Wuite, J., Floricioiu, D., Nagler, T., Scheiblauer, S., 2015. Synergy of TanDEM-X DEM differencing and input-output method for glacier monitoring, in: 2015 IEEE International Geoscience and Remote Sensing Symposium (IGARSS). Presented at the 2015 IEEE International Geoscience and Remote Sensing Symposium (IGARSS), pp. 5216–5219. doi:10.1109/IGARSS.2015.7327010

Scambos, T., Hulbe, C., Fahnestock, M., 2003. Climate-Induced Ice Shelf Disintegration in the Antarctic Peninsula, in: Domack, E., Levente, A., Burnet, A., Bindschadler, R., Convey, P., Kirby, tthew (Eds.), Antarctic Peninsula Climate Variability: Historical and Paleoenvironmental Perspectives. American Geophysical Union, pp. 79–92.

Scambos, T.A., Berthier, E., Haran, T., Shuman, C.A., Cook, A.J., Ligtenberg, S.R.M., Bohlander, J., 2014. Detailed ice loss pattern in the northern Antarctic Peninsula: widespread decline driven by ice front retreats. The Cryosphere 8, 2135–2145. doi:10.5194/tc-8-2135-2014

Scambos, T.A., Bohlander, J., Shuman, C.A., Skvarca, P., 2004. Glacier acceleration and thinning after ice shelf collapse in the Larsen B embayment, Antarctica. Geophys. Res. Lett. 31. doi:10.1029/2004GL020670

Seehaus, T., Marinsek, S., Helm, V., Skvarca, P., Braun, M., 2015. Changes in ice dynamics, elevation and mass discharge of Dinsmoor–Bombardier–Edgeworth glacier system, Antarctic Peninsula. Earth Planet. Sci. Lett. 427, 125–135. doi:10.1016/j.epsl.2015.06.047

Seehaus, T.C., Marinsek, S., Skvarca, P., van Wessem, J.M., Reijmer, C.H., Seco, J.L., Braun, M.H., 2016. Dynamic Response of Sjögren Inlet Glaciers, Antarctic Peninsula, to Ice Shelf Breakup Derived from Multi-Mission Remote Sensing Time Series. Front. Earth Sci. 4. doi:10.3389/feart.2016.00066

Skvarca, P., Rack, W., Rott, H., Donángelo, T.I., 1999. Climatic trend and the retreat and disintegration of ice shelves on the Antarctic Peninsula: an overview. Polar Res. 18, 151–157.

Skvarca, P., Rack, W., Rott, H., Ibarzábal y Donángelo, T., 1998. Evidence of recent climatic warming on the eastern Antarctic Peninsula. Ann. Glaciol. 27, 628–632.

Skvarca, P., Rott, H., Nagler, T., 1995. Satellite imagery, a base line for glacier variation study on James Ross Island, Antarctica. Ann. Glaciol. 21, 291–296.

Strozzi, T., Luckman, A., Murray, T., Wegmuller, U., Werner, C.L., 2002. Glacier motion estimation using SAR offset-tracking procedures. IEEE Trans. Geosci. Remote Sens. 40, 2384–2391. doi:10.1109/TGRS.2002.805079

Thomas, E.R., Marshall, G.J., McConnell, J.R., 2008. A doubling in snow accumulation in the western Antarctic Peninsula since 1850. Geophys. Res. Lett. 35. doi:10.1029/2007GL032529

Turner, J., 2002. Spatial variability of Antarctic Peninsula net surface mass balance. J. Geophys. Res. 107. doi:10.1029/2001JD000755

Turner, J., Colwell, S.R., Marshall, G.J., Lachlan-Cope, T.A., Carleton, A.M., Jones, P.D., Lagun, V., Reid, P.A., Iagovkina, S., 2005. Antarctic climate change during the last 50 years. Int. J. Climatol. 25, 279–294. doi:10.1002/joc.1130

Turner, J., Lu, H., White, I., King, J.C., Phillips, T., Hosking, J.S., Bracegirdle, T.J., Marshall, G.J., Mulvaney, R., Deb, P., 2016. Absence of 21st century warming on Antarctic Peninsula consistent with natural variability. Nature 535, 411–415. doi:10.1038/nature18645

van Lipzig, N.P.M., King, J.C., Lachlan-Cope, T.A., van den Broeke, M.R., 2004. Precipitation, sublimation, and snow drift in the Antarctic Peninsula region from a regional atmospheric model. J. Geophys. Res. Atmospheres 109, D24106. doi:10.1029/2004JD004701

van Lipzig, N.P.M., Meijgaard, E. van, Oerlemans, J., 2002. The spatial and temporal variability of the surface mass balance in Antarctica: results from a regional atmospheric climate model. Int. J. Climatol. 22, 1197–1217. doi:10.1002/joc.798

van Wessem, J.M., Ligtenberg, S.R.M., Reijmer, C.H., van de Berg, W.J., van den Broeke, M.R., Barrand, N.E., Thomas, E.R., Turner, J., Wuite, J., Scambos, T.A., van Meijgaard, E., 2016. The modelled surface mass balance of the Antarctic Peninsula at 5.5 km horizontal resolution. The Cryosphere 10, 271–285. doi:10.5194/tc-10-271-2016

van der Veen, C.J., 2002. Calving glaciers. Prog. Phys. Geogr. 26, 96–122. doi:10.1191/0309133302pp327ra

Walker, K.-M., Zenone, C., 1988. Multitemporal Landsat multispectral scanner and thematic mapper data of the Hubbard Glacier region, southeast Alaska. Photogramm. Eng. Remote Sens. 54, 373–376.

Ward, J.H., 1963. Hierarchical Grouping to Optimize an Objective Function. J. Am. Stat. Assoc. 58, 236–244. doi:10.1080/01621459.1963.10500845

Wendt, J., Rivera, A., Wendt, A., Bown, F., Zamora, R., Casassa, G., Bravo, C., 2010. Recent ice-surface-elevation changes of Fleming Glacier in response to the removal of the Wordie Ice Shelf, Antarctic Peninsula. Ann. Glaciol. 51, 97–102.

Wuite, J., Rott, H., Hetzenecker, M., Floricioiu, D., De Rydt, J., Gudmundsson, G.H., Nagler, T., Kern, M., 2015. Evolution of surface velocities and ice discharge of Larsen B outlet glaciers from 1995 to 2013. The Cryosphere 9, 957–969. doi:10.5194/tc-9-957-2015

Figures

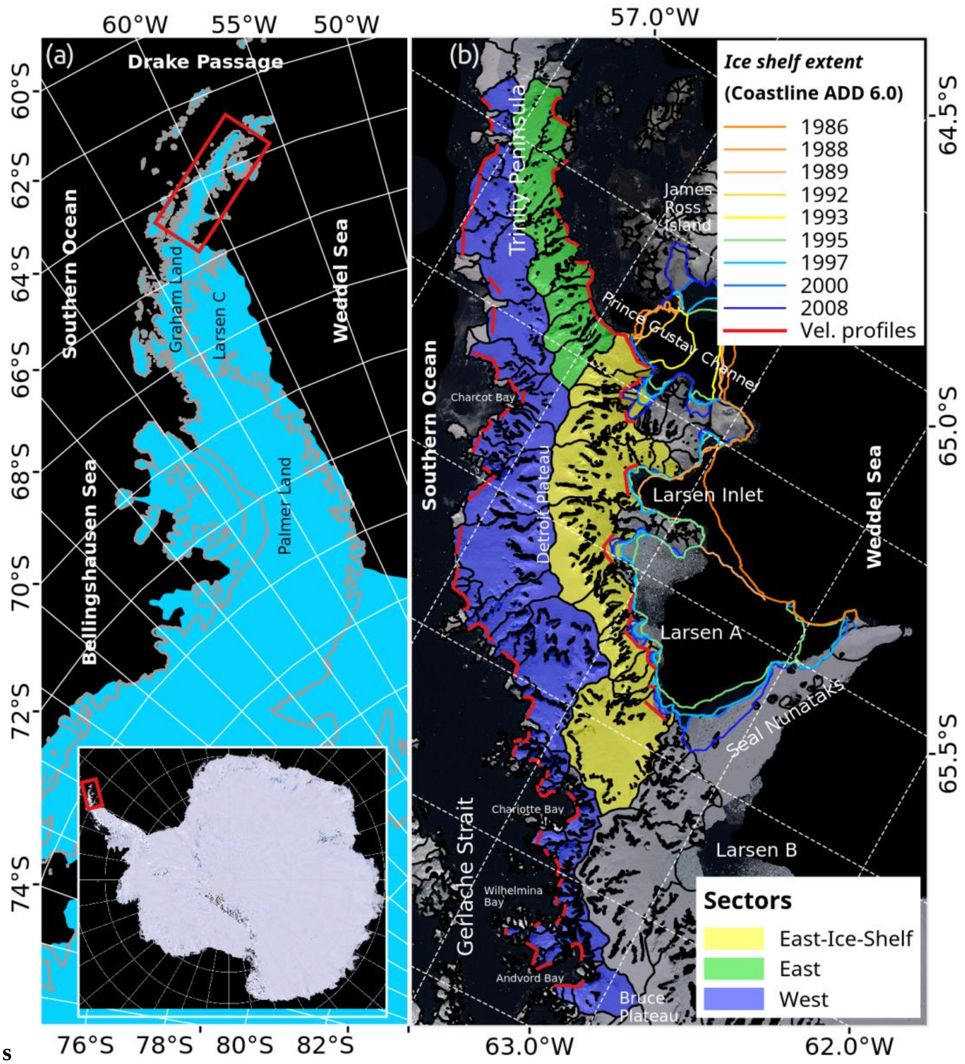

s

Figure 1. Panels **(a)** Location of study site on the Antarctic Peninsula and on the Antarctic continent (inset). Panel **(b)**. Separation of study site in 3 sectors and retreat states of Prince-Gustav and Larsen A ice shelves. Red lines: profiles at glacier front for velocity measurements. Map base, Landsat LIMA Mosaic © USGS, NASA, BAS, NSF, coastlines (ice shelf extent) and catchment delineations from SCAR Antarctic Digital Database 6.0.

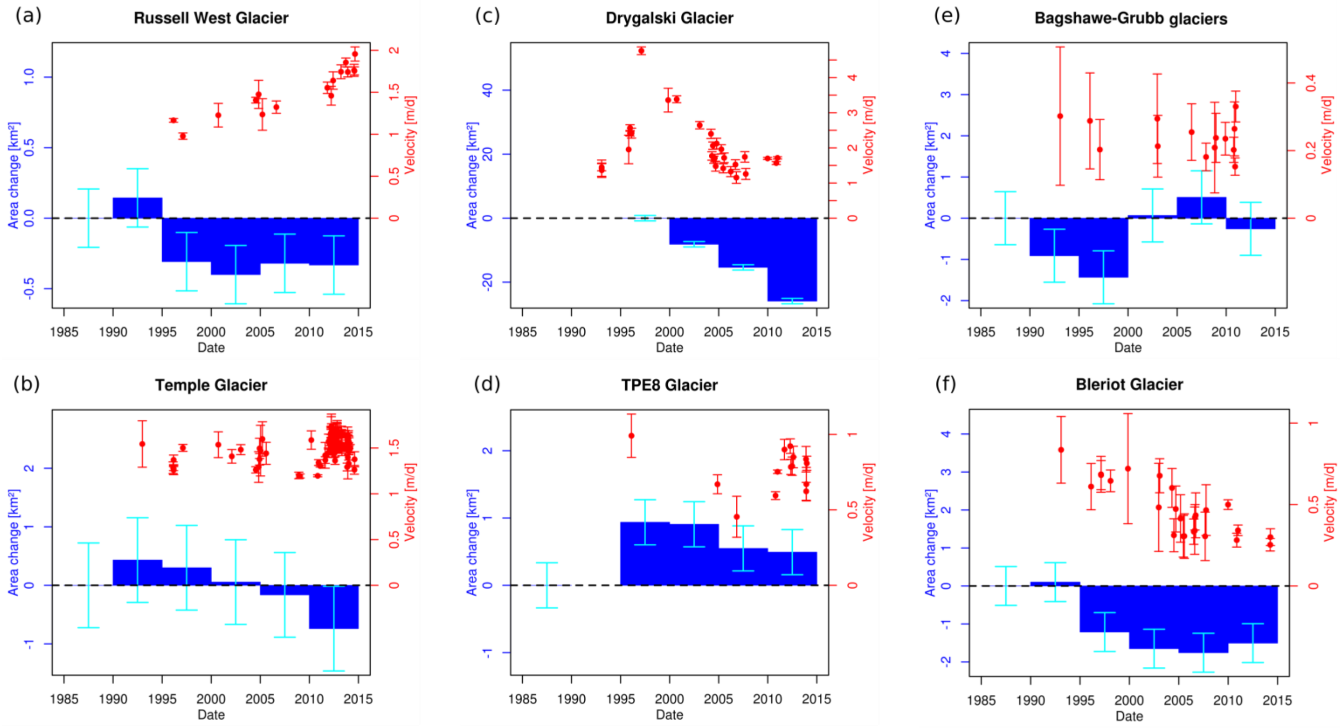

Figure 2. Temporal trend of surface velocity (red) and area (blue) changes of selected glaciers in the study region for each velocity change category (see Table 3).

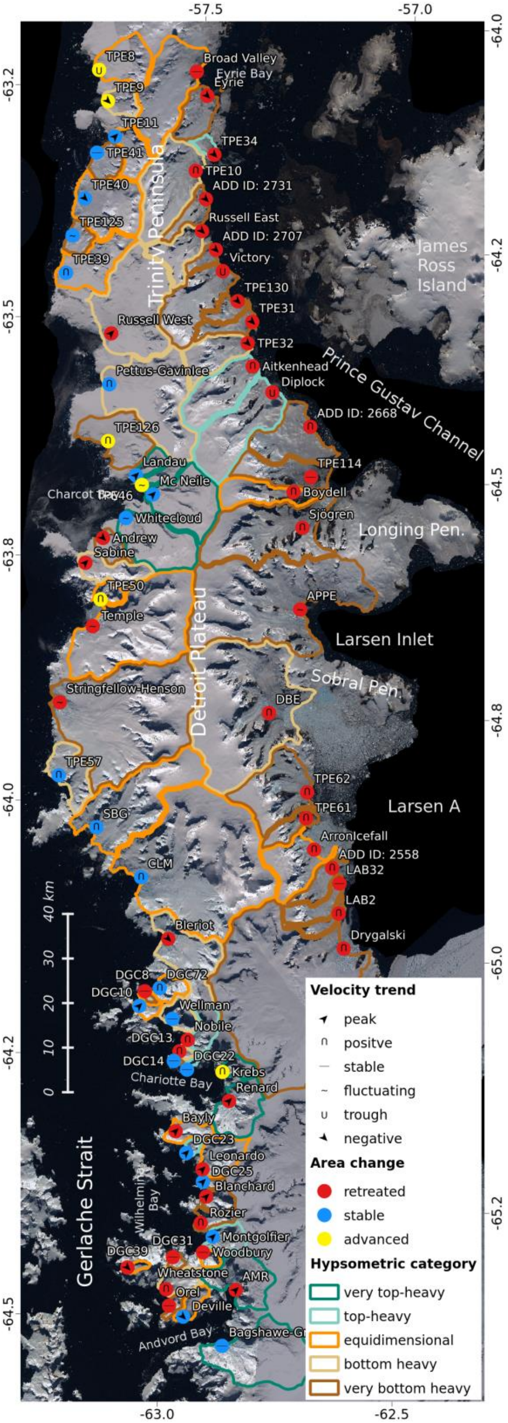

Trinity Peninsula
Detroit Plateau
James Ross Island
Prince Gustav Channel
Longing Pen.
Larsen Inlet
Sobral Pen.
Larsen A
Gerlache Strait
Wilhelmina Bay
Charlotte Bay
Andvord Bay
TPE8
TPE9
TPE11
TPE41
TPE40
TPE125
TPE39
Broad Valley
Eyrie Bay
Eyrie
TPE34
TPE10
ADD ID: 2731
Russell East
ADD ID: 2707
Victory
TPE130
TPE31
TPE32
Russell West
Pettus-GavinIce
Aitkenhead
Diplock
ADD ID: 2668
TPE126
Landau
Mc Neile
Charcot Bay
TPE46
Whitecloud
TPE114
Boydell
Sjogren
Andrew
Sabine
TPE50
Temple
APPE
Stringfellow-Henson
DBE
TPE57
TPE62
TPE61
SBG
ArronIcefall
ADD ID: 2558
LAB32
LAB2
CLM
Drygalski
Bleriot
DGC8
DGC72
DGC10
Wellman
Nobile
DGC13
DGC14
DGC22
Krebs
Renard
Bayly
DGC23
Leonardo
DGC25
Blanchard
Rozier
DGC31
Montgolfier
DGC39
Woodbury
Wheatstone
AMR
Orel
Deville
Bagshawe-Gr
40 km
30
20
10
0
Velocity trend
peak
positve
stable
fluctuating
trough
negative
Area change
retreated
stable
advanced
Hypsometric category
very top-heavy
top-heavy
equidimensional
bottom heavy
very bottom heavy
-57.5
-57.0
-63.0
-62.5
-63.2
-63.5
-63.8
-64.0
-64.2
-64.5
-64.0
-64.2
-64.5
-64.8
-65.0
-65.2

Figure 3. Categorizations of glaciers to temporal trends in area changes (dots) and flow velocities (symbols). Colors of catchment delineation indicate Hypsometric categories according to Jiskoot et al. (2009). Background: Landsat LIMA Mosaic © USGS, NASA, BAS, NSF

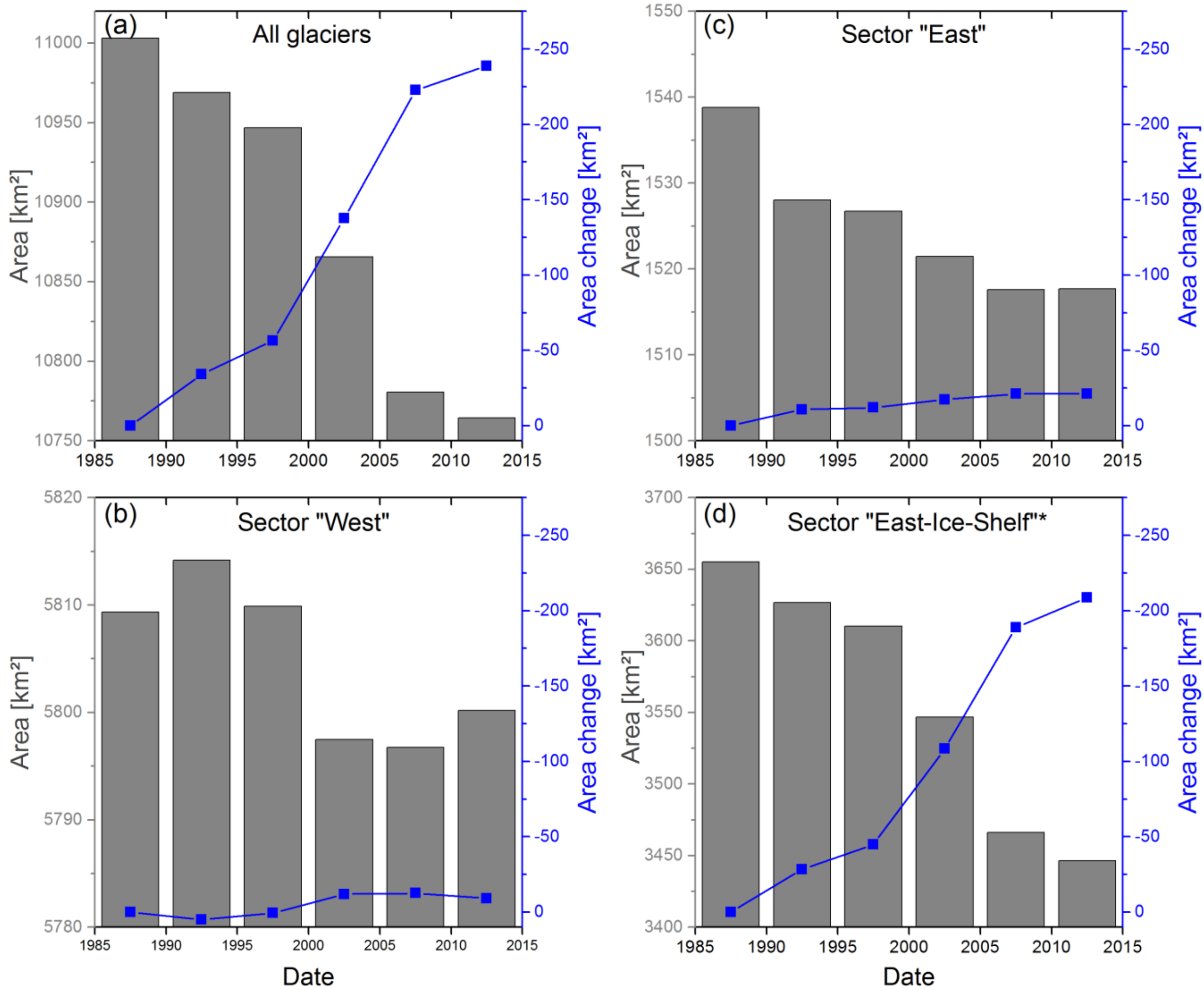

Figure 4. Total glacier area (gray bars) of the whole study site (Panel **(a)**) and of the individual sectors (Panels **(b)**-**(d)**) in the period 1985-2015. Changes in glacier area (blue points) are relative to the measurements in time interval 1985-1990. Note the different scaling of the lest y-axes. In sector "East", area changes before 1995 are only measured at Larsen Inlet tributaries (APPE glaciers).

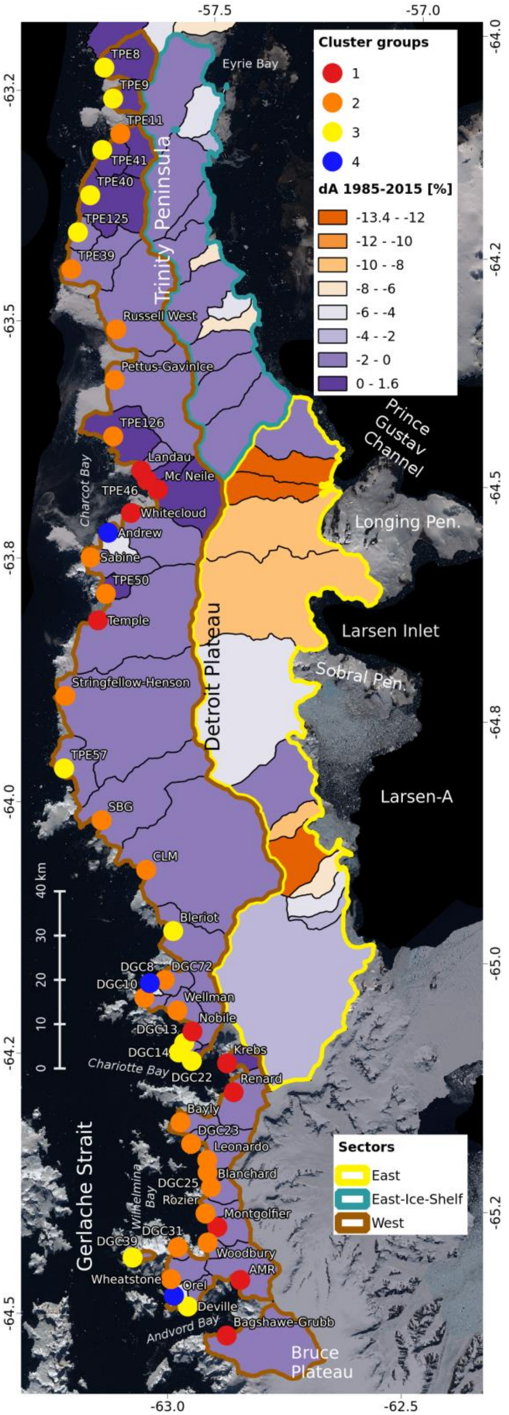

Figure 5. Spatial distribution of glacier types along the west coast. Glaciers are group based on a hierarchical cluster analysis (dots). In Section 5.3 the characteristics of the groups are discussed in detail. Individual glacier catchment colors: relative area change in the period

1985-2015. Colored polygon outlines: Boundaries of the three regional sectors. Background: Landsat LIMA Mosaic © USGS, NASA, BAS, NSF

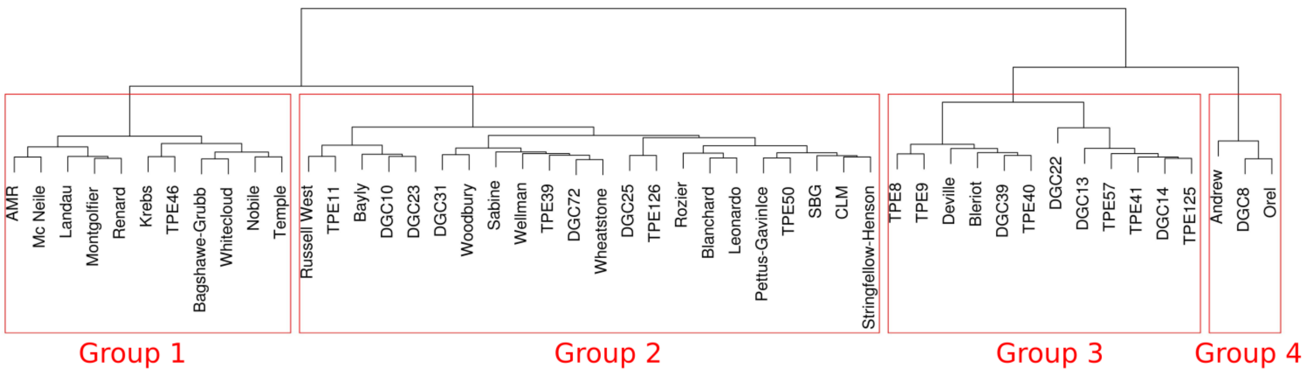

Figure 6. Dendrogram of hierarchical cluster analysis of glaciers in sector "West". The glaciers are assorted in four groups (red rectangles). See also Section 5.3.

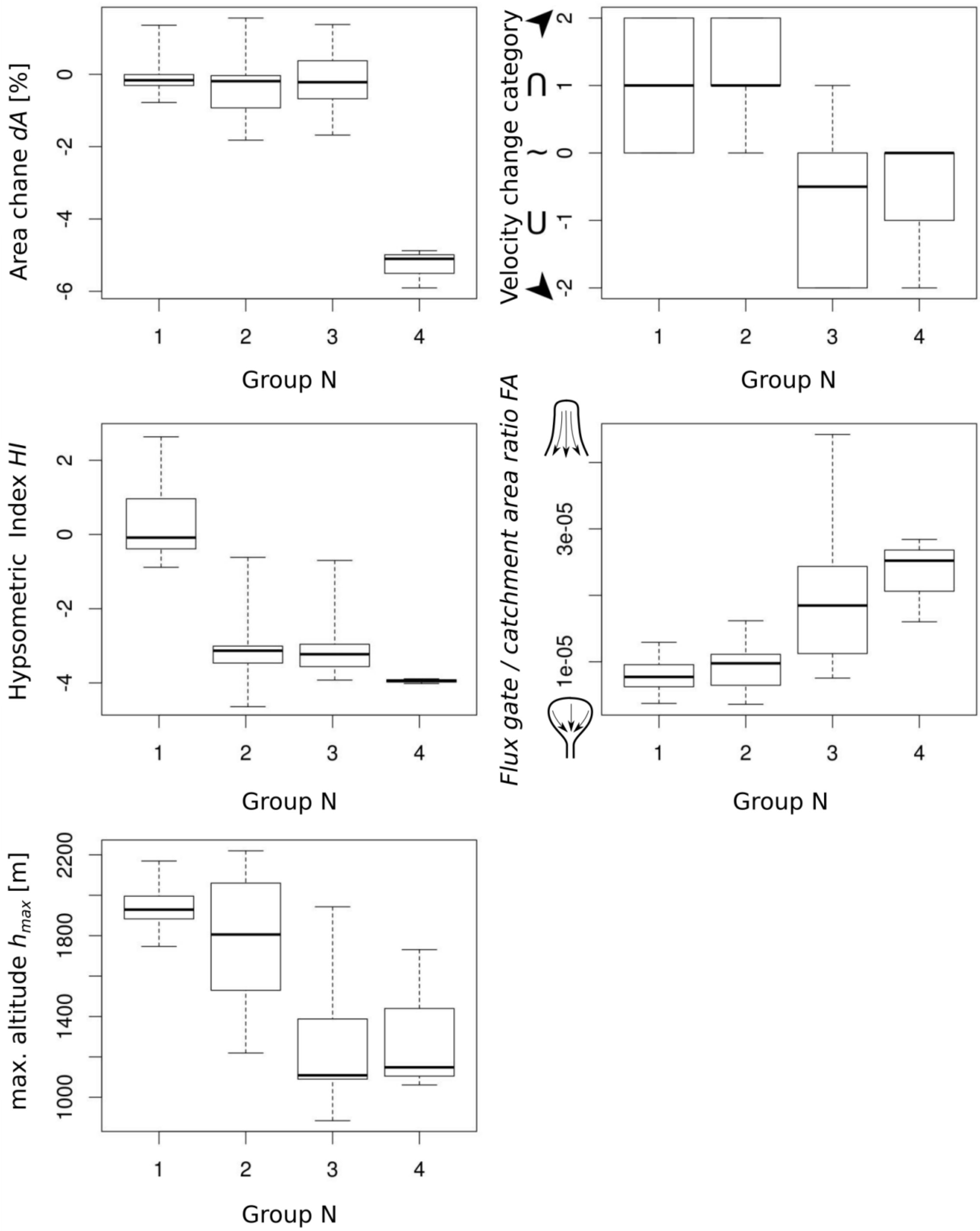

Figure 7. Boxplots of cluster analysis input variables (Sector "West") for each group. Whiskers extend to the most extreme data points.

Tables

Table 1. Abbreviations of glacier names

Abbreviation	Glacier names
AMR	Arago-Moser-Rudolph
APPE	Albone-Pyke-Polaris-Eliason
CLM	Cayley-Lilienthal-Mouillard
DBE	Dinsmoor-Bombardier-Edgeworth
SBG	Sikorsky-Breguet-Gregory

Table 2. Overview of SAR sensors and specifications used in this study.

Platform	Sensor	Mode	SAR band	Repetition cycle [d]	Time interval	Ground range resolution [m]*	Tracking patch sizes [p x p]+	Tracking step size [p x p]+	Mean uncertainty of tracking results [m/d]
ERS-1/2	SAR	IM	C band	35/1	08. December 1992 02. April 2010	30	48x240 64x320	5x25	0.15±0.10
RADARSAT 1	SAR	ST	C band	24	10. September 2000 03. September 2006	30	48x192 64x256	5x20	0.11±0.03
Envisat	ASAR	IM	C band	35	05. December 2003 16. August 2009	30	32x160 64x320 128x640	5x25	0.12±0.05
ALOS	PALSAR	FBS	L band	46	18. May 2006 17. March 2011	10	64x192 96x192 128x384	10x30	0.05±0.06
TerraSAR-X TanDEM-X	SAR	SM	X band	11	14. October 2008 22. December 2014	3	128x128 256x256 512x512	25x25	0.06±0.04

* nominal resolution; depending on the incidence angle.

+ Intensity tracking parameters are provided in pixels [p] in slant range geometry.

Table 3. Description of velocity change categories.

Category	Description	Rating*
positive	General increase of flow speed	2
peak	Increase of flow speed with subsequent deceleration	1
stable	Variability of measurements < 0.25 m d^{-1}	0
fluctuating	Short term speed-ups and deceleration, no clear trend	0
trough	Decrease of flow speed with subsequent acceleration	-1
negative	General decrease of flow speed	-2

*Ratings used for cluster analysis Section 3.4

Table 4. Hypsometric Index and glacier basin category descriptions.

Hypsometric Index (HI)*	Hypsometric categories	Number of Glaciers
$HI < -1.5$	Very top-heavy	8
$-1.5 < HI < -1.2$	Top-heavy	7
$-1.2 < HI < 1.2$	Equidimensional	18
$1.2 < HI < 1.5$	Bottom-heavy	13
$HI > 1.5$	Very bottom-heavy	28

*according to Jiskoot et al., (2009)

Table 5. Summary of observed parameters for each sector and all glaciers.

Sector	East	East-Ice-Shelf	West	All glaciers
N	13	13	48	74
l_f [m]	85114	127909	268763	481786
$A_{1985-1990}$ [km²]	1538.78	3655.13	5809.33	11003.23
$A_{2010-2015}$ [km²]	1517.71	3446.54	5800.18	10764.42
dA [km²]	-21.07	-208.59	-9.14	-238.81
dt [a]	18.79	19.05	20	19
v_S [m d^{-1}]	0.995	0.480	0.427	0.537
v_E [m d^{-1}]	0.307	0.561	0.605	0.545
dv [m d^{-1}]	-0.688	0.081	0.177	0.008
n_v	319	584	1600	2503

N – number of studied glaciers

l_f – length of ice front

A – Glacier area in the respective period (subscript)

dA – Change in glacier area between 1985 and 2015

dt: mean time period of velocity measurements

v_S – mean of earliest velocity measurements (1992-1996)

v_E – mean of latest velocity measurements (2010-2014)

dv – mean velocity change

n_v – sum of velocity measurements in the observation period (dt)